Journal of Molecular Structure 983 (2010) 12–21

Contents lists available at ScienceDirect

Journal of Molecular Structure

journal homepage: www.elsevier.com/locate/molstruc

Vibrational spectra and first-order molecular hyperpolarizabilities of p-hydroxybenzaldehyde dimer

D. Sajan [a,c,*], Y. Erdogdu [b], Thomas Kuruvilla [a], I. Hubert Joe [c]

[a] Department of Physics, Bishop Moore College, Mavelikara, Alappuzha 690 110, Kerala, India
[b] Department of Physics, Ahi Evran University, 40040 Kirsehir, Turkey
[c] Centre for Molecular and Biophysics Research, Department of Physics, Mar Ivanios College, Thiruvananthapuram 695 015, Kerala, India

ARTICLE INFO

Article history:
Received 13 May 2010
Received in revised form 31 July 2010
Accepted 2 August 2010
Available online 6 August 2010

Keywords:
NIR-FT-Raman spectroscopy
FT-IR spectroscopy
DFT
ICT

ABSTRACT

Single crystals of p-hydroxybenzaldehyde (PHBA) were grown by the slow evaporation technique and vibrational spectral analysis was carried out using near-IR Fourier transform Raman and Fourier transform IR spectroscopy. The density functional theoretical (DFT) computations were also performed at the B3LYP/6-311++G(d,p) level to derive the equilibrium geometry, vibrational wavenumbers and intensities. The detailed interpretation of the vibrational spectra has been carried out with the aid of normal coordinate analysis (NCA) following the scaled quantum mechanical force field methodology. The various intramolecular interactions that is responsible for the stabilization of the molecule was revealed by natural bond orbital analysis. Vibrational analysis based on the NIR-FT-Raman, FT-IR and computed spectrum reveals that the CH in-plane bending of the aldehyde group interacts with its stretching mode via Fermi Resonance and evidence for intermolecular interaction can be well identified as two CH bands in IR spectra at 2740 and 2804 cm^{-1} aldehyde group of the p-hydroxybenzaldehyde dimer. The red shift of the O–H stretching wavenumber is due to the formation of strong O–H···O hydrogen bonds by hyperconjugation between the carbonyl oxygen lone electron pairs and the O–H σ^* anti-bonding orbitals.

1. Introduction

The search for new materials with non-linear optical (NLO) properties has been the subject of intense research due to their application in a wide range of technologies such as optical computing and optical communication [1,2]. In the past years much attention has been paid to organic NLO materials due to their promising applications in optoelectronics technology [3,4], their large nonlinear response, extremely fast switching time and convenient optimization routes through molecular engineering compared to the currently studied inorganic materials [5]. It has been generally understood that for a material to have useful and highly efficient NLO properties, the constituting molecules need first to exhibit large molecular hyperpolarizabilities, which are generally characterized by a highly extended π-conjugated chain with strong electron donor–acceptor pairs at the ends (D–π–A) [6]. Since a large molecular hyperpolarizability β is the basis of a strong second harmonic generation (SHG) response; organic molecules with long conjugation systems that usually exhibit large β values are certainly candidate molecules for NLO materials.

The benzaldehyde and substituted benzaldehydes have been subjected to various spectroscopic studies [7–24]. Mono-, halo-, methoxy and ethoxy-substituted benzaldehydes, among others, have attracted the attention of the spectroscopists. *o*- and *m*-Chlorobenzaldehydes have been shown to have *trans* and *cis* conformers by Matrix Isolation IR spectroscopy [25]. Vibrational spectral studies of the molecules can provide deeper knowledge about the relationships between molecular architecture, non-linear response, and hyperpolarizability and support the efforts towards discovery of new efficient materials for technological applications. NIR-FT-Raman spectroscopy combined with quantum chemical computations have recently been used as effective tools in the vibrational analysis of drug molecules, biological compounds natural products and NLO active compounds [26–30], since fluorescence free Raman spectra and computed results can help unambiguous identification of vibrational modes as well as the bonding and structural features of complex organic molecular systems. The present work deals with detailed vibrational spectral investigation of p-hydroxybenzaldehyde (PHBA) dimer (Fig. 1) molecules using NIR-FT-Raman and FT-IR spectra, along with density functional theoretical computations to study the structural and bonding features, nature of hydrogen bonding and vibrational

* Corresponding author at: Department of Physics, Bishop Moore College, Mavelikara, Alappuzha 690 110, Kerala, India. Tel.: +91 9495043765; fax: +91 4792303230.
E-mail address: dsajand@gmail.com (D. Sajan).

0022-2860/$ - see front matter © 2010 Elsevier B.V. All rights reserved.
doi:10.1016/j.molstruc.2010.08.003

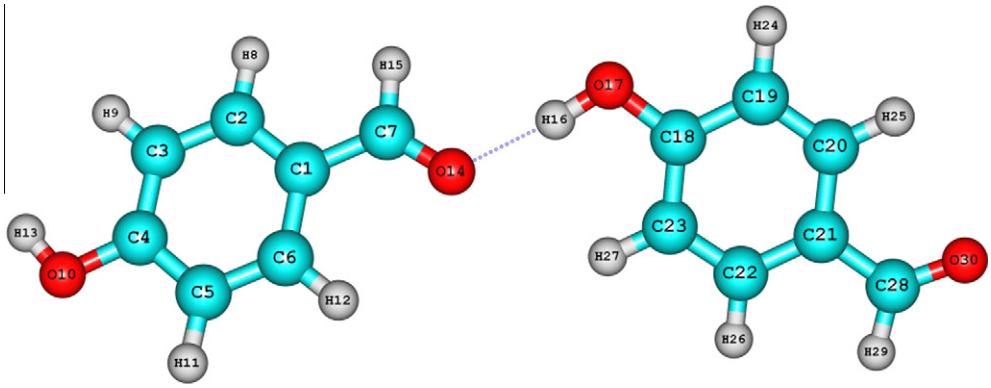

Fig. 1. Optimized structure of PHBA dimer calculated at B3LYP/6-31++G(d,p).

interactions of the molecule supported by scaled quantum mechanical (SQM) force field calculations.

2. Materials and methods

2.1. Sample preparation

The title compound 4-hydroxybenzaldehyde (98% Aldrich) was obtained from Sigma–Aldrich and was recrystallized from ethylacetate by slow evaporation [31] to obtain good quality crystals.

2.2. IR and Raman measurements

The FT-IR spectrum of PHBA was recorded using Perkin Elmer RXI spectrometer in the region 4000–500 cm^{-1}, with samples in the KBr. The resolution of the spectrum is 2 cm^{-1}. The NIR-FT-Raman spectrum of PHBA crystal was obtained in the range 3500–10 cm^{-1} using Bruker RFS 100/S FT-Raman spectrophotometer with a 1064 nm Nd: YAG laser source of 100 mW power. Liquid nitrogen cooled Ge-diode was used as a detector. Spectra were collected for samples with 1000 scan accumulated for over 30 min duration. The spectral resolution after apodization was 2 cm^{-1}.

3. Computational methods

The DFT computations has been used to calculate the equilibrium structures of PHBA in the form of Becke's three-parameter exchange functional in combination with the Lee, Yang and Parr (LYP) correlation functional (B3LYP) combined with split valence basis sets 6-311++G(d,p). Equilibrium molecular geometry was fully optimized and harmonic vibrational wavenumber analysis was then performed to confirm the minima on the potential energy surface. All calculations were performed using the Gaussian'09 program package [32]. In order to assist assignments of vibrational modes, the theoretical infrared and Raman spectra were calculated. The calculated vibrational wavenumbers were scaled [33] with the scale factors in order to figure out how the calculated data were in agreement with those of the experimental ones. The vibrational modes were assigned on the basis of PED analysis using Scaled Quantum Mechanics (SQM) program [34]. The infrared intensities were calculated on the basis of the dipole moment derivatives with respect to the Cartesian coordinates. The Raman activities (S_i) calculated by the Gaussian-09 program have been converted to relative Raman intensities (I_i) using the following relationship derived from the basic theory of Raman scattering [35,36].

$$I_i = \frac{f(\nu_o - \nu_i)^4 S_i}{\nu_i[1 - \exp(\frac{-hc\nu_i}{kT})]} \quad (1)$$

where ν_o is the exciting frequency (in cm^{-1} units), ν_i is the vibrational wavenumber of the ith normal mode, hc and k are universal constants, and f is the suitably chosen common scaling factor for all the peak intensities. The simulated IR and Raman spectra have been plotted using pure Lorentzian band shapes with full width at half maximum (FWHM) of 10 cm^{-1}.

4. Results and discussion

4.1. Crystal structure

PHBA crystallizes in space group $P2_{1/C}$. From the single crystal XRD data [31] it is observed that the crystal belongs to monoclinic system with the following cell dimensions: a = 6.6992 Å, b = 13.5550 Å, c = 7.1441 Å, $\alpha = \gamma = 90°$, β = 112.871°. Crystal packing is stabilized by intermolecular O–H···O interactions between the hydroxyl and aldehyde groups which link the molecules into chains in a zigzag pattern along the [1 1 0] plane of the unit cell.

4.2. Optimized geometry

The optimized geometrical parameters are given in Table 1 with the comparison of the XRD data. The global minimum energy of PHBA monomer and dimer calculated by DFT structure optimization method is −420.9188 Hartrees and −841.8522 Hartrees, respectively. The molecules in PHBA dimer (Fig. 1) are bound together via O_{17}–H_{16}···O_{14} hydrogen-bonded interaction. This interaction arises largely through the one equivalent stable hydrogen bonded O_{17}–H_{16}···O_{14} and contacts that result in increased stabilization. By examining Table 1 it becomes evident that O17–H_{16} (0.016 Å) and C_7=O_{14} (0.01 Å) bonds are significantly elongated while C_{18}–O_{17} bonds are shortened. The shortening of the C_{18}–O_{17} bond (single) upon dimerization is due to the redistribution of partial charges on the O atoms as the unpaired electron is significantly delocalized and thereby the C_{18}–O_{17} bond shows considerable double bond character typical of a carbonyl group. The intermolecular hydrogen bond O_{17}–H_{16}···O_{14} is 1.793 Å which is slightly lower as compared to that reported values [31]. The optimized geometry shows that OH and CHO groups substituted in para position of phenyl ring which predicts maximum conjugation of molecule with donor and acceptor groups. The C_{18}–O_{17} [1.348 Å] and C_1–C_7 [1.460 Å] bond lengths are only slightly shorter than normal C–O and C–C single bonds, indicating conjugation between the two aromatic ring systems.

Table 1
Optimized Geometry of PHBA monomer and dimmer by B3LYP/6-31++G(d,p) in comparison with XRD data.

Bond length (°)				Bond angle (°)				Torsion angle (°)			
Parameter	Values			Parameter	Values			Parameter	Values		
	Monomer	Dimer	XRD		Monomer	Dimer	XRD		Monomer	Dimer	XRD
C_1–C_2	1.402	1.401	1.395	C_1–C_2–C_3	120.78	120.71	119.35	C_1–C_2–C_3–C_4	0.0034	0.0112	0.7
C_1–C_6	1.383	1.407	1.395	C_2–C_3–C_4	119.41	119.39	121.50	C_2–C_3–C_4–C_5	−0.0004	−0.0046	−0.8
C_1–C_7	1.474	1.46	1.448	C_3–C_4–C_5	120.44	120.51	118.39	C_3–C_4–C_5–C_6	−0.0023	−0.0036	−0.2
C_2–C_3	1.383	1.387	1.374	C_4–C_5–C_6	119.62	119.63	120.61	C_7–C_1–C_2–C_3	179.99	−179.83	−179.78
C_2–H_8	1.086	1.085	0.930	C_2–C_1–C_6	119.11	119.2	120.02	H_8–C_2–C_3–C_4	−180	−179.96	−178.88
C_3–C_4	1.398	1.399	1.395	C_6–C_1–C_7	121.06	121.26	122.62	H_9–C_3–C_4–C_5	179.99	−179.98	178.76
C_3–H_9	1.086	1.085	0.930	C_7–C_1–C_2	119.84	119.54	119.9	O_{10}–C_4–C_5–C_6	179.99	−179.98	−179.85
C_4–C_5	1.402	1.404	1.395	H_8–C_2–C_3	119.62	119.63	120.3	H_{11}–C_5–C_6–C_1	−180.00	−179.96	−179.25
C_4–O_{10}	1.361	1.356	1.354	H_9–C_3–C_4	120.1	120.13	120.3	H_{12}–C_6–C_1–C_2	180.00	−179.92	179.23
C_5–C_6	1.383	1.381	1.372	O_{10}–C_4–C_5	117.01	116.87	117.30	H_{13}–O_{10}–C_4–C_3	−0.0482	0.0169	−4.96
C_5–H_{11}	1.083	1.083	0.930	O_{10}–C_4–C_3	122.56	122.62	122.68	O_{14}–C_7–C_1–C_6	0.0045	0.2198	3.34
C_6–H_{12}	1.084	1.083	0.930	H_{11}–C_5–C_6	121.59	121.62	119.9	H_{15}–C_7–C_1–C_2	0.0112	0.1223	2.38
O_{10}–H_{13}	0.964	0.964	0.930	H_{12}–C_6–C_1	118.6	118.81	119.9	H_{15}–C_7–O_{14}–H_{16}	–	3.1178	−158.31
C_7–O_{14}	1.213	1.223	1.219	H_{13}–O_{10}–C_4	110.2	110.54	104.4	C_7–$O_{14}\cdots H_{16}$–O_{17}	–	12.258	−76.20
C_7–H_{15}	1.111	1.107	0.930	O_{14}–C_7–C_1	125.22	124.83	126.7	$O_{14}\cdots H_{16}$–O_{17}–C_{18}	–	−174.96	−149.55
C_{18}–O_{17}	1.361	1.348	1.354	H_{15}–C_7–C_1	114.44	115.29	116.7				
$O_{14}\cdots H_{16}$	–	1.793	1.92	O_{14}–C_7–H_{15}	120.34	119.87	116.7	–	–	–	–
H_{16}–O_{17}	0.964	0.98	0.82	$O_{14}\cdots H_{16}$–O_{17}	–	174.13	171.0	–	–	–	–
$O_{14}\cdots O_{17}$	–	2.769	2.731	–	–	–	–	–	–	–	–

4.3. Conformational analysis

In order to reveal all possible conformations of PHBA, a detailed potential energy surface (PES) scan in C_7–C_2–O_1–H_{15} and C_5–C_{12}–O_{14}–H_{15} dihedral angles was performed (Fig. 2). The scan was carried out by minimizing the potential energy in all geometrical parameters by changing the torsion angle every 10° for 180° rotation around the bond. The shape of the potential energy as a function of the dihedral angle is illustrated in Fig. 3.

The energy of monomer 1 is predicted at −420.918973677 a.u. (relative energy is at 0 kJ mol^{-1}) by B3LYP/6-311++G(d,p) level of theory. The relative energy of monomer 3 is determined at 0.385 kJ mol^{-1}. The energy of monomer 2 is predicted at −420.888 761785 a.u. According to monomer 2, the relative energy of monomer 4 is determined at 0.709 kJ mol^{-1}. The monomer 1 is the most stable because of their high energy (Fig. 2).

4.4. Natural bond orbital analysis

NBO analysis is proved to be an effective tool for chemical interpretation of hyperconjugative interaction and electron density transfer (EDT) from filled lone electron pairs of the n(Y) of the "Lewis base" Y into the unfilled anti-bond σ^* (X–H) of the "Lewis acid" X–H in X–H···Y hydrogen bonding systems [37]. NBO analysis has been performed on PHBA dimer in order to elucidate intermolecular hydrogen bonding, intermolecular charge transfer (ICT), rehybridization, delocalization of electron density and cooperative effect due to $n(O) \rightarrow \sigma^*$ (O–H). The intermolecular O–H···O hydrogen

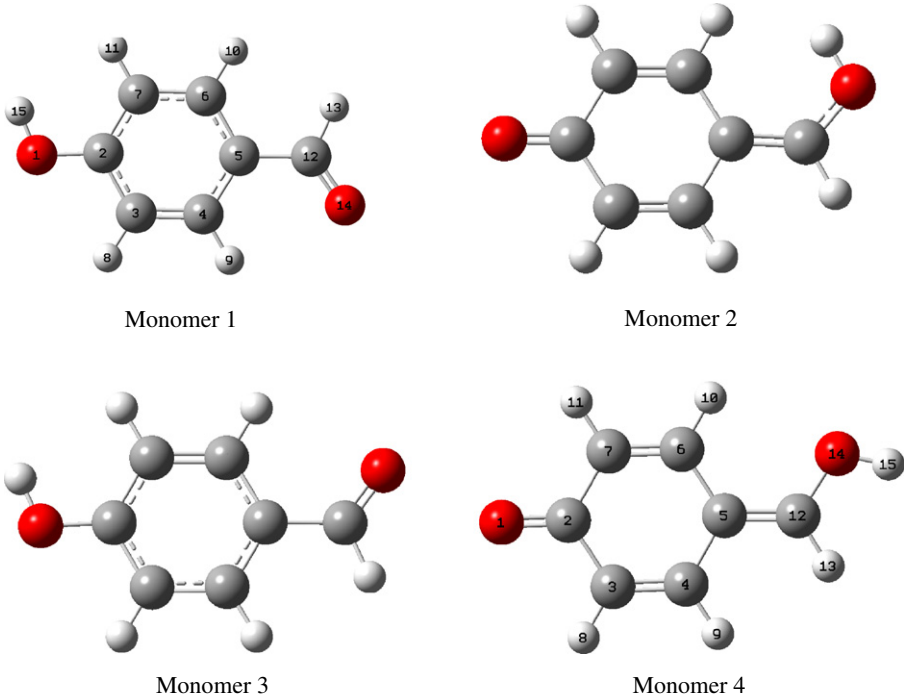

Fig. 2. Optimized structure of all conformer of PHBA calculated at B3LYP/6-31++G(d,p).

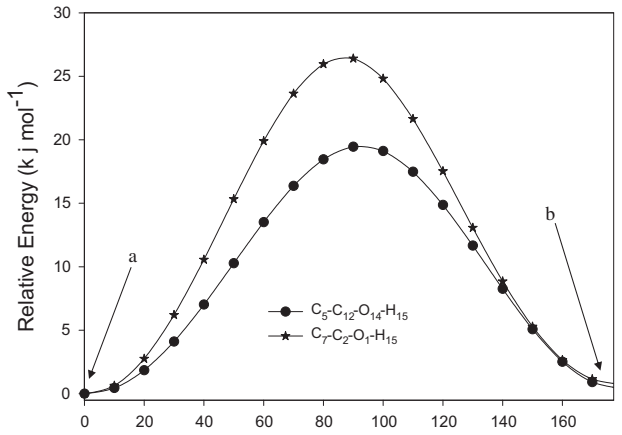

Fig. 3. Potential energy surface scan for dihedral angles C_7–C_2–O_1–H_{15} and C_5–C_{12}–O_{14}–H_{15}. (a) Monomers 1 and 2. (b) Monomers 3 and 4.

bonding is formed by the orbital overlap between the n(O) and σ^* (O–H) which results ICT causing stabilization of the H-bonded systems. Hence hydrogen bonding interaction leads to an increase in electron density (ED) of O–H anti-bonding orbital. The increase of population in O–H anti-bonding orbital weakens the O–H bond. Thus the nature and strength of the intermolecular hydrogen bonding can be explored by studying the changes in electron densities in vicinity of O···H hydrogen bonds.

The NBO analysis of PHBA in comparison between monomer and dimer clearly manifests the evidences of the formation strong H-bonded interactions between oxygen lone electron pairs and σ^* (O–H) anti-bonding orbitals. The magnitudes of charges transferred from lone pair of $n(O_{17})$ of the hydrogen bonded O atoms into the anti-bonds σ^* (O_{17}–H_{16}) being the H-donors, respectively was significantly increased (0.05099e and 0.0479e) upon dimerisation providing unambiguous evidence about the weakening of both bonds, their elongation and concomitant red shifts of their stretching wavenumber. Similar conclusion can be obtained while considering the energy of each orbital. The stabilization energy $E(2)$ associated with hyperconjugative interactions $n_1(O_{14}) \rightarrow \sigma^*$ (O_{16}–H_{17}) and $n_2(O_{14}) \rightarrow \sigma^*$ (O_{16}–H_{17}) are obtained as 6.05 and 18.02 kcal mol^{-1}, respectively (Table 2) which quantify the extend of intermolecular hydrogen bonding. The differences in $E(2)$ energies are reasonably due to the fact that the accumulation of electron density in the O–H bond is not only drawn from the n(O) of hydrogen-acceptor but also from the entire molecule. Further, the second order perturbation theory analysis of Fock matrix in NBO basis shows that the $n_2(O_{14})$ and $n_1(O_{14})$ can readily interact with the σ^* (C_7–H_{15}) and σ^* (C_{23}–H_{27}) anti-bonding orbitals, respectively. H-bonded NBO in terms of natural atomic hybrids also demonstrates that the redistribution of natural charges in the O–H bonds as the hydrogen side of the bond becomes less positive (−0.00585e at H_{16}) which destabilizes the H-bond. Because hyperconjugation and rehybridization act in opposite directions, the compression and elongation of the bond O–H is a result of a balance of the two effects. However the hyperconjugative interaction is dominant and overshadows the rehybridization effect resulting a significant elongation in O–H bond (0.01853 Å) and a concomitant red shift in stretching wavenumber.

Table 2
Second order perturbation theory analysis of Fock matrix in NBO basis.

Donor (i)	Acceptor (j)	$E(2)$[a] (kcal mol^{-1})	$E(j)$–$E(i)$[b] (a.u.)	$F(i,j)$[c] (a.u.)
Within unit 1				
$n_1(O_{10})$	σ^* (C_3–C_4)	6.55	1.15	0.064
$n_2(O_{10})$	π^* (C_3–C_4)	32.31	0.35	0.101
$n_1(O_{14})$	σ^* (C_7–H_{15})	3.21	1.10	0.053
$n_1(O_{14})$	σ^* (C_1–C_7)	17.36	0.79	0.106
$n_2(O_{14})$	σ^* (C_7–H_{15})	15.44	0.72	0.096
From unit 1 to unit 2				
$n_1(O_{14})$	σ^* (H_{16}–O_{17})	6.05	1.15	0.075
$n_1(O_{14})$	σ^* (C_{23}–H_{27})	0.11	1.19	0.010
$n_2(O_{14})$	σ^* (H_{16}–O_{17})	18.02	0.77	0.107
Within unit 2				
$n_1(O_{17})$	σ^* (O_{18}–C_{19})	0.73	1.11	0.025
$n_1(O_{17})$	σ^* (O_{18}–C_{23})	7.31	1.11	0.081
$n_2(O_{17})$	π^* (O_{18}–C_{23})	34.97	0.34	0.103
$n_1(O_{30})$	σ^* (C_{21}–C_{28})	1.86	1.16	0.042
$n_1(O_{30})$	σ^* (C_{28}–H_{29})	1.05	1.09	0.031
$n_1(O_{30})$	σ^* (C_{21}–C_{28})	18.71	0.73	0.016
$n_2(O_{30})$	σ^* (C_{28}–H_{29})	22.36	0.67	0.111

[a] $E(2)$ means energy of hyperconjugative interactions.
[b] Energy difference between donor and acceptor i and j NBO orbitals.
[c] $F(i,j)$ is the Fock matrix element between i and j NBO orbitals.

4.5. Vibrational spectra

The vibrational spectral assignments have been carried out with the help of normal coordinate analysis. The detailed vibrational assignments of fundamental modes along with the calculated IR and Raman intensities and normal mode description (characterized by PED) are reported in Table 3. For visual comparison, the observed and simulated FT-IR and FT-Raman spectra are presented in Figs. 4 and 5, respectively.

4.5.1. Hydroxyl group vibrations

The hydroxyl stretching and bending bands can be identified by the breadth and strength of the band, which are dependent on the extent of hydrogen bonding [38–40]. The non-hydrogen bonded or free hydroxyl group absorbs strongly in the 3700–3584 cm^{-1} region while the existence of intermolecular hydrogen bond formation can lower the O–H stretching wavenumber to the 3550–3200 cm^{-1} region. The DFT computations give the wavenumber of this band at 3343 cm^{-1} for the O–H stretch. The O–H stretching vibration appears at 3165 cm^{-1} as strong IR band with slight broadness, which reveals the presence of strong intermolecular hydrogen bond network. The appearance of the red shift of the O_{16}–H_{17} stretching wavenumber is clearly due to the formation of a O–H···O hydrogen bond. Interaction of lone pairs of oxygen (electron donor) with the O–H anti-bonding σ^* orbital leads to an increase of electron populations in this orbital, followed by a weakening of the O–H bond which is accompanied by a lowering of the O–H stretching wavenumber, which is justified by the natural bond orbital analysis (Table 3).

DFT calculation shows that the OH in-plane bending vibrations are mixed with the C–C–H bending and C–C stretching vibrations. The band corresponding to OH in-plane bend is identified in the IR and Raman spectrum around at 1451 cm^{-1}. The O–H out-of-plane bending vibration gives rise to a broad band in the region 700–600 cm^{-1}. The position of this band is dependant on the strength of the hydrogen bond the stronger the hydrogen bond, the higher the wavenumbers. The broad band at 698 cm^{-1} in the infrared spectrum is attributed to the O–H out-of-plane bending mode. In presence of hydrogen bonding, the characteristic weak band due to the out-of-plane bending mode of C–O–H bend is observed [38–42] at 450–350 cm^{-1}. The band correlated with the out-of-plane bending mode of the C–O–H mode was identified at 338 cm^{-1} in the Raman spectra. Similar band positions of the out-of-plane bending mode of the C–O–H mode have been observed for other molecules with intermolecular hydrogen bonding [24]. Hence, the bands position of the C–O–H may serve as a sensitive measure of the strength of the interaction between the O–H group and the lone pair electron of the neighboring oxygen atom.

Table 3
Observed and calculated wavenumbers (cm^{-1}), PED and assignment for PHBA dimer at B3LYP/6-311++G(d,p) level.

DIMER B3LYP/6-311++G(d,p)			MONOMER B3LYP/6-311++G(d,p)			Exp. IR	Exp. Raman	Assignments	PED[d] (%)
Scaled wavenumbers[a]	I_{IR} [b]	I_{Raman} [c]	Scaled wavenumbers[a]	I_{IR} [b]	I_{Raman} [c]				
11	0.014	0.119						C–O–H–O torsion	$\Gamma_{C18-O17-H16-O14}(100)$
12	0.057	0.103						O–H–C o.p bend + O–H–O o.p bend	$\gamma_{H16-O14-C7}(47)$, $\gamma_{O17-H16-O14}(46)$
15	0.073	0.110						H–O–C–C torsion + O–H–O–C torsion	$\Gamma_{H-O-C-C}(58)$, $\Gamma_{O-H-O-C}(38)$, $\Gamma_{C-C-O-H}(11)$
45	0.062	0.078						C–C–O–H torsion + O–H–O–C torsion	$\Gamma_{C-C-O-H}(58)$, $\Gamma_{O-H-O-C}(19)$, $\Gamma_{H-O-C-C}(16)$
55	0.022	0.713						O–O stretch + O–H–C o.p bend	$\upsilon_{O14-O17}(12)$, $\gamma_{H-O-C}(51)$, $\gamma_{O-H-O}(24)$
91	0.174	0.294					93 s	O–O stretch + C–C–C o.p bend	$\upsilon_{O14-H16-O17}(56)$, $\gamma_{C-C-C}(10)$
99	0.176	0.443	96	0.526	0.195		108 s	C–C–C–O torsion + C–C–C–C torsion	$\Gamma_{C-C-C-O}(26)$, $\Gamma_{C-C-C-C}(23)$
112	0.024	0.505					121 w	H–O–C–C torsion + C–C–C–O torsion	$\Gamma_{H-O-C-C}(25)$, $\Gamma_{C-C-C-O}(17)$, $\Gamma_{C-C-C-C}(17)$
189	0.219	0.018	185	2.199	0.996		181 w	C–C–C–O torsion + H–C–C–O torsion	$\Gamma_{C-C-C-O}(38)$, $\Gamma_{H-C-C-C}(13)$
190	0.245	0.490						C–C–C–O torsion + H–C–C–C torsion	$\Gamma_{C-C-C-O}(52)$, $\Gamma_{H-C-C-C}(16)$
194	0.306	1.150	193	1.546	0.350			C–C–C o.p bend + C–C–O o.p bend	$\gamma_{C-C-C}(65)$, $\gamma_{C-C-O}(11)$
231	1.076	2.458					223 w	C–C–C o.p bend + O–H stretch	$\upsilon_{O-H}(20)$, $\gamma_{C-C-C}(50)$
313	0.035	0.209	313	0.295	0.173			C–C–C–C torsion + C–C–C–O torsion + H–C–C–C torsion	$\Gamma_{C-C-C-C}(23)$, $\Gamma_{C-C-C-O}(22)$, $\Gamma_{H-C-C-C}20)$
315	0.185	0.024						C–C–C–O torsion + C–C–C–C torsion + H–C–C–C torsion	$\Gamma_{C-C-C-O}(22)$, $\Gamma_{C-C-C-C}(23)$, $\Gamma_{H-C-C-C}(22)$
368	5.237	6.624	347	36.78	0.677		338 w	H–O–C–C torsion	$\Gamma_{H-O-C-C}(94)$
388	0.982	40.22	378	0.975	1.606			C–C stretch + C–C–O o.p bend + C–C–C o.p bend	$\upsilon_{C-C}(13)$, $\gamma_{C-C-O}(46)$, $\gamma_{C-C-C}(14)$
390	0.053	18.23						C–C stretch + C–C–O o.p bend + C–C–C o.p bend	$\upsilon_{C-C}(27)$, $\gamma_{C-C-C}(39)$, $\gamma_{C-C-O}(15)$
414	0.081	13.01	411	0.528	1.027			C–C–C–C torsion + C–C–C–H torsion	$\Gamma_{C-C-C-C}(60)$, $\Gamma_{C-C-C-H}(17)$
417	0.045	0.554						C–C–C–C torsion + C–C–C–H torsion	$\Gamma_{C-C-C-C}(59)$, $\Gamma_{C-C-C-H}$ (21)
417	0.559	0.328	413	6.644	21.21		416 m	C–C–C o.p bend + C–C–O o.p bend + C–C stretch	6a $\gamma_{C-C-C}(37)$, $\gamma_{C-C-O}(36)$, $\upsilon_{C-C}(12)$
440	0.137	1.411					452 w	C–C–O o.p bend	$\gamma_{C-C-O}(56)$
499	0.846	0.066	497	5.144	3.061			C–C–C–H torsion + C–C–C–C torsion + O–C–C–C torsion	$\Gamma_{C-C-C-H}$ (46), $\Gamma_{C-C-C-C}(21)$, $\Gamma_{O-C-C-C}(11)$
501	0.587	0.219						C–C–C–H torsion + C–C–C–C torsion	$\Gamma_{C-C-C-H}$ (52), $\Gamma_{C-C-C-C}(19)$
598	1.628	0.359	597	8.594	4.682			C–C–C o.p bend + C–C–O o.p bend	$\gamma_{C-C-C}(24)$, $\gamma_{C-C-O}(20)$
602	2.139	2.736				603 vs	604 m	C–C–C o.p bend + C–C–O o.p bend	6b$\gamma_{C-C-C}(32)$, $\gamma_{C-C-O}(19)$
630	0.017	0.669						C–C–C o.p bend	$\gamma_{C-C-C}(38)$
631	0.784	6.785	631	0.437	37.61	641s	645 m	C–C–C o.p bend	4 $\gamma_{C-C-C}(36)$
684	0.364	0.398	671	0.012	2.764			C–C–C–H torsion + C–C–C–C torsion	$\Gamma_{C-C-C-C}(43)$, $\Gamma_{C-C-C-H}(19)$
692	0.807	0.071				698 sbr		C–C–C–C torsion + O–H–O–C torsion + C–C–C–H torsion	$\Gamma_{C-C-C-C}(29)$, $\Gamma_{O-H-O-C}(15)$, $\Gamma_{C-C-C-H}(11)$
715	2.688	3.157						H–O–C–C torsion + C–C–C–C torsion	$\Gamma_{O-H-C-C}(34)$, $\Gamma_{H-O-C-C}(15)$, $\Gamma_{C-C-C-C}(13)$
772	0.355	6.430						C–C stretch + C–O stretch + C–C–C o.p bend + C–C–O o.p bend	$\upsilon_{C-C}(27)$, $\upsilon_{C-O}(13)$, $\gamma_{O-C-C}(13)$, $\gamma_{C-C-C}(19)$
774	0.412	2.396	768	1.422	7.420			C–C stretch + C–O stretch + O–C–C o.p bend + C–C–C o.p bend	$\upsilon_{C-C}(25)$, $\upsilon_{C-O}(15)$, $\gamma_{O-C-C}(12)$, $\gamma_{C-C-C}(22)$
788	1.196	8.636	782	10.29	0.605	789 s	792 w	C–C–C–H torsion + H–C–C–O torsion	$\Gamma_{C-C-C-H}(64)$, $\Gamma_{H-C-C-O}(25)$
804	0.974	0.352						C–C–C–H torsion + H–C–C–O torsion	$\Gamma_{C-C-C-H}(65)$, $\Gamma_{H-C-C-O}(20)$
825	2.309	3.301	821	9.891	0.446			C–C–C–H torsion + H–C–C–O torsion	$\Gamma_{C-C-C-H}(56)$, $\Gamma_{H-C-C-O}(24)$
827	0.910	3.518						C–C–C–H torsion + H–C–C–O torsion	$\Gamma_{C-C-C-H}(47)$, $\Gamma_{H-C-C-O}(28)$
835	1.117	0.280	834	10.77	100	832 vs	836 w	C–C stretch	1 $\upsilon_{C-C}(72)$
837	1.414	1.407				859 s	862 m	C–C stretch	12 $\upsilon_{C-C}(71)$
917	0.014	0.183	904	0.278	0.207			C–C–C–H torsion + H–C–C–O torsion	$\Gamma_{C-C-C-H}(56)$, $\Gamma_{H-C-C-O}(24)$
922	0.000	0.067						C–C stretch	$\upsilon_{C-C}(66)$
958	0.001	0.026	960	0.000	0.683	945 w		C–C–C–H torsion + H–C–C–H torsion	$\Gamma_{C-C-C-H}(34)$, $\Gamma_{H-C-C-H}(40)$
962	0.001	0.188						C–C–C–H torsion + H–C–C–H torsion	$\Gamma_{C-C-C-H}(42)$, $\Gamma_{H-C-C-H}(38)$
988	0.003	3.580						C–C–C o.p bend + C–C stretch + C–C–H o.p bend	$\gamma_{C-C-C}(31)$, $\upsilon_{C-C}(32)$, $\gamma_{C-C-H}(32)$

988	0.012	1.283	989	0.005	0.564			C–C–C o.p bend + C–C stretch + C–C–H o.p bend	$\gamma_{C-C-C}(31)$, $\upsilon_{C-C}(32)$, $\gamma_{C-C-H}(32)$
991	0.057	1.002	993	0.489	4.774			C–C–C–H torsion + H–C–C–O torsion	$\Gamma_{C-C-C-H}(67)$, $\Gamma_{C-C-C-O}(24)$
998	0.047	0.184				1009 w	1014 w	C–C–C–H torsion + H–C–C–O torsion	$\Gamma_{C-C-C-H}(66)$, $\Gamma_{C-C-C-O}(22)$
1088	0.323	4.292	1087	3.950	1.456			C–C stretch + C–C–H i.p bend	$\delta_{C-C-H}(56)$, $\upsilon_{C-C}(23)$
1090	0.678	10.12				1113 s		C–C stretch + C–C–H i.p bend	18b $\delta_{C-C-H}(54)$, $\upsilon_{C-C}(23)$
1140	10.24	0.016	1140	61.98	37.44			C–C stretch + C–C–H i.p bend	$\delta_{C-C-H}(67)$, $\upsilon_{C-C}(23)$
1141	11.03	19.70						C–C stretch + C–C–H i.p bend	$\delta_{C-C-H}(59)$, $\upsilon_{C-C}(20)$
1151	3.683	1.919	1152	36.84	5.253	1159 vs	1163 vs	C–C stretch + C–C–H i.p bend + C–O–H i.p bend	18a $\delta_{C-H}(19)$, $\upsilon_{C-C}(22)$, $\delta_{C4-O10-H13}(49)$
1194	6.027	0.616	1191	17.14	32.56			C–C stretch + C–C–H i.p bend	$\upsilon_{C-C}(57)$, $\delta_{C-C-H}(23)$
1204	5.550	3.370						C–C stretch + C–C–H i.p bend	$\upsilon_{C-C}(53)$, $\delta_{C-C-H}(19)$
1225	9.015	3.913				1217 vs	1218 s	Ring stretch + C–C–H i.p bend + C–O–H i.p bend	15 $\delta_{C-C-H}(19)$, $\upsilon_{C-C}(30)$, $\delta_{C18-O17-H16}(16)$
1258	8.176	19.00	1248	45.20	14.17	1240 m	1238 vwsh	Ring stretch + C–C–H i.p bend + C–O stretch	$\upsilon_{C-O}(52)$, $\delta_{C-H}(12)$, $\upsilon_{C-C}(18)$
1271	7.453	2.607						Ring stretch + C–C–H i.p bend + C–O stretch	$\upsilon_{C-O}(47)$, $\delta_{C-C-H}(23)$, $\upsilon_{C-C}(18)$
1286	1.369	2.232						Ring stretch + C–C–H i.p bend +	$\delta_{C-C-H}(45)$, $\upsilon_{C-C}(28)$
1288	1.992	33.73	1283	11.12	1.092	1284 vs	1286 m	Ring stretch + C–C–H i.p bend +	3 $\delta_{C-C-H}(61)$, $\upsilon_{C-C}(14)$
1333	0.956	45.03	1328	7.285	2.864	1315 s	1315 m	Ring stretch + C–O–H i.p bend	14 υ_{C-C} (63), $\delta_{H13-O10-C4}(19)$
1362	5.284	4.592						Ring stretch + C–C–H i.p bend + C–O–H i.p bend	$\upsilon_{C-C}(45)$, $\delta_{C-C-H}(15)$, $\delta_{C18-O17-H16}(25)$
1373	0.097	25.87						C–C–H i.p bend + C–O–H i.p bend	$\delta_{C-C-H}(31)$, $\delta_{O30-C28-H29}(47)$
1378	0.352	3.112	1374	1.150	1.238	1387 m	1395 vw	C–C–H i.p bend + C–O–H i.p bend	$\delta_{C-H}(28)$, $\delta_{O14-C7-H15}(44)$
1425	0.363	1.651	1423	0.288	4.149	1423 vwsh	1422 vvw	Ring stretch + C–C–H i.p bend +	19b $\upsilon_{C-C}(34)$, $\delta_{C-C-H}(29)$
1437	1.051	0.573				1452 vs	1451 m	Ring stretch + C–C–H i.p bend + C–O–H i.p bend	$\upsilon_{C-C}(28)$, $\delta_{C-C-H}(26)$, $\delta_{C-O-H}(21)$
1492	2.360	5.030	1489	11.59	2.429			Ring stretch + C–H i.p bend	$\upsilon_{C-C}(33)$, $\delta_{C-C-H}(46)$
1494	2.412	23.20				1518 m		Ring stretch + C–H i.p bend	19a $\upsilon_{C-C}(41)$, $\delta_{C-C-H}(47)$
1559	22.38	11.01						Ring stretch	$\upsilon_{C-C}(64)$
1564	3.341	3.144	1567	41.59	24.39			Ring stretch	8b $\upsilon_{C-C}(64)$
1589	25.29	100						Ring stretch	$\upsilon_{C-C}(65)$
1590	2.451	89.41	1592	63.80	65.08	1583 vvs	1586 vvs	Ring stretch	8a $\upsilon_{C-C}(64)$
1669	24.06	2.450				1665 vs	1666 vs	C=O stretch	$\upsilon_{C7=O14}(79)$
1693	13.46	0.073	1703	100	64.71			C=O stretch	$\upsilon_{C28=O30}(85)$
2741	5.831	1.431	2749	39.50	13.19	2789 w	2790 w	Aldehyde C–H stretch	$\upsilon_{C28-H29}(99)$
						2831 w		Aldehyde C–H stretch	υ_{C-H}
2804	2.712	0.784				2879 w	2880 w	Aldehyde C–H stretch	$\upsilon_{C7-H15}(99)$
3013	0.391	3.638	3011	3.580	4.086	3016 wsh	3021 w	Aromatic C–H stretch	$7\upsilon_{C-H}(99)$
3017	0.401	1.730						Aromatic C–H stretch	$\upsilon_{C-H}(99)$
3031	0.336	0.970	3027	2.900	7.294	3044 w	3043 w	Aromatic C–H stretch	20b $\upsilon_{C-H}(99)$
3038	0.076	0.677						Aromatic C–H stretch	$\upsilon_{C-H}(99)$
3040	0.174	0.354	3044	0.053	2.660		3066 w	Aromatic C–H stretch	20a $\upsilon_{C-H}(98)$
3047	0.005	10.14						Aromatic C–H stretch	$\upsilon_{C-H}(99)$
3052	0.240	4.404						Aromatic C–H stretch	$\upsilon_{C-H}(99)$
3060	0.118	4.593	3057	1.105	7.945	3088 vwsh	3094 vw	Aromatic C–H stretch	2 $\upsilon_{C-H}(99)$
3343	100	4.782				3165 sbr		O–H stretch	$\upsilon_{O17-H16}(100)$
3651	4.868	4.971	3654	28.43	3.996			O–H stretch	$\upsilon_{O10-H13}(100)$

υ – Stretch, δ – in-plane bending, γ – o.p plane bending, Γ – torsion.

[a] Obtained from the wavenumbers calculated at B3LYP/6-31++G(d,p) using scaling factors 0.967 (for wavenumbers under 1800 cm^{-1}) and 0.955 (for those over 1800 cm^{-1}).

[b] Relative absorption intensities normalized with highest peak absorption equal to 100.

[c] Relative Raman intensities calculated by Eq. (1) and normalized to 100.

[d] (Dimer forms) Total energy distribution calculated B3LYP/6-311++G(d,p) level of theory. Only contributions ⩾10% are listed.

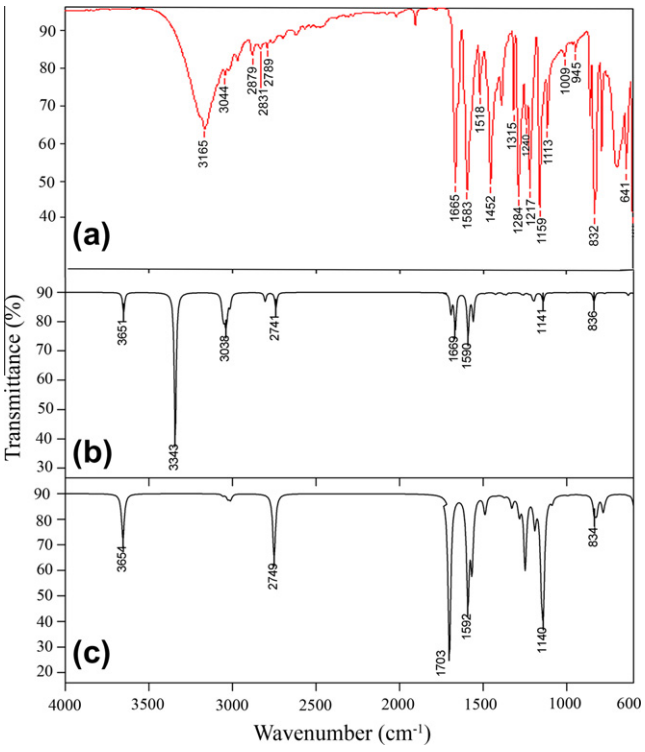

Fig. 4. (a) FT-IR spectra of PHBA (b) simulated IR spectra of PHBA dimer and (c) simulated IR spectra of PHBA monomer.

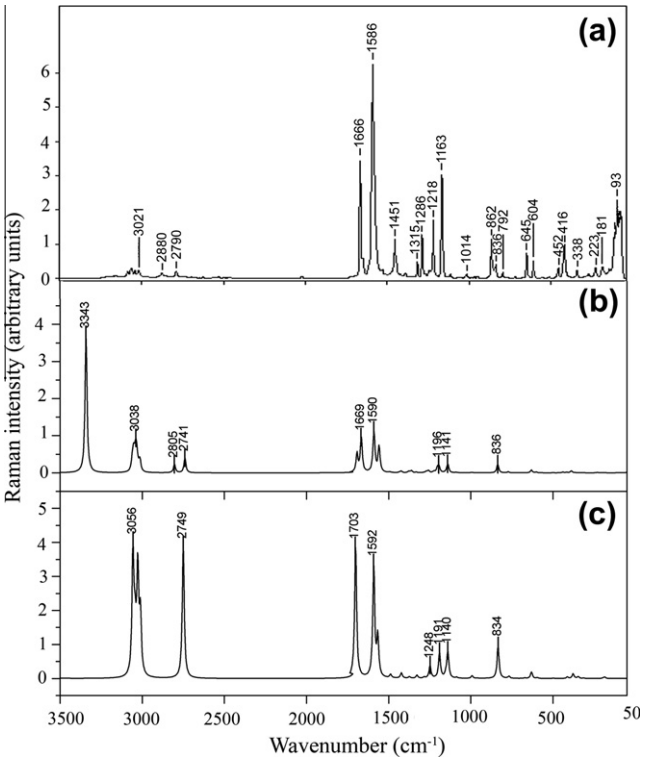

Fig. 5. (a) FT-Raman spectra of PHBA (b) simulated Raman spectra of PHBA dimer and (c) simulated Raman spectra of PHBA monomer.

4.5.2. Vibrations of aldehyde group

The aldehyde C–H stretching vibration can be distinctly observed in both IR and Raman spectra, by its band position in the low wavenumber region, compared to other C–H stretching vibrations. The C–H stretching vibration of aldehyde group can occur in the region 2900–2700 cm^{-1} in the benzaldehye derivatives [7–24]. DFT computation provides the C–H stretching vibrations of PHBA dimer associated with the wavenumbers at 2741 and 2804 cm^{-1}, respectively. The weak IR bands at 2879 and 2789 cm^{-1} may be considered as first overtone of 1452 cm^{-1} and combination band (1452 + 1387) cm^{-1}, respectively. The shift of band position can be attributed to the possible interactions of C–H stretching mode with the overtone of C–H in-plane bending, which reduces the intensity of C–H stretching band via Fermi resonance [10–20]. Therefore we confirmed that these two bands are the partners in the C–H doublet of PHBA.

Though the DFT computation gives the C=O stretching wavenumber to be 1669 cm^{-1}, the conjugation of C=O bond with the phenyl ring is expected to lower the stretching wavenumber to 1665 cm^{-1}, evident from the NBO analysis. The C=O stretching vibration is further influenced by intermolecular hydrogen bonding between aldehyde group and hydroxyl group (Fig. 1). The above two features are additive and the band position is further lowered to produce very strong band in IR at 1665 cm^{-1} and a very strong Raman band at 1666 cm^{-1}. The C–O stretching vibrations in alcohols and phenols produce a strong band in the 1260–1000 cm^{-1} of the spectrum. The C–O stretching mode is coupled with the adjacent C–C stretching vibration and hence these modes can be described as an asymmetric C–C–O stretching vibration. The medium IR band at 1240 cm^{-1} corresponds to the C–O stretching vibration are coupled with C–H in-plane bending and C–C stretching modes. The $\Gamma_{C-C-C-O}$ vibrations manifest as weak IR bands at 1009 cm^{-1}, which is coupled with $\Gamma_{C-C-C-H}$ vibrations.

4.5.3. Phenyl ring vibrations

The aromatic structure shows the presence of C–H stretching vibrations in the region 3000/3100 cm^{-1} which is the characteristic region for ready identification of this structure [38–41]. In this region, the bands are not affected appreciably by the nature of the substituents. In benzene derivatives, the C/H stretching wavenumber arise from the modes a_{1g} (3062 cm^{-1}), e_{2g} (3047 cm^{-1}), b_{1u} (3060 cm^{-1}) and e_{1u} (3080 cm^{-1}). The weak Raman band at 3094 cm^{-1} with weak IR absorption at 3088 cm^{-1} is assigned to mode 2 of benzene, which corresponds to the aromatic C–H stretching. The weak infrared band at 3016 cm^{-1} and the corresponding weak Raman band at 3021 cm^{-1} have major contribution from 7b. The C–H stretching mode 20a observed on the low wavenumber side of benzene mode 2, can be found as a weak shoulder in Raman spectrum at 3066 cm^{-1}. The weak Raman band at 3043 cm^{-1} and the corresponding weak band in IR band at 3044 $cm^{-1}$is attributed to the C–H stretching mode 20b. These assignments are in good agreement with PED results also.

The ring stretching vibrations are very much prominent in the spectrum of benzene and its derivatives are highly characteristic of the aromatic ring itself. Benzene has two doubly degenerate vibrations e_{2g} (1596 cm^{-1}) and e_{1u} (1485 cm^{-1}) [41]. On the removal of the degeneracy, the components of this vibration appear separately (8a, 8b) [38–41]. DFT computation gives the vibrational modes 8a and 8b at wavenumbers, 1590 cm^{-1} and 1564 cm^{-1} and such a splitting cannot be observed experimentally which is contrary to the selection rule allowed for p-disubstituted phenyl ring. The degeneracy of mode 8 remains unperturbed and the mode 8a appears in both IR and Raman with equal and high strength at 1583 cm^{-1} and 1586 cm^{-1}, respectively. This can be interpreted as the result of intermolecular charge transfer between π-electron donor (OH group) and acceptor (CHO group) via conjugated path which contributes to the hyperpolarizability enhancement of the PHBA. The appearance of ring mode 8 with equal intensity in IR and Raman can be considered as a strong vibrational spectral evidence of intramolecular charge transfer and subsequent

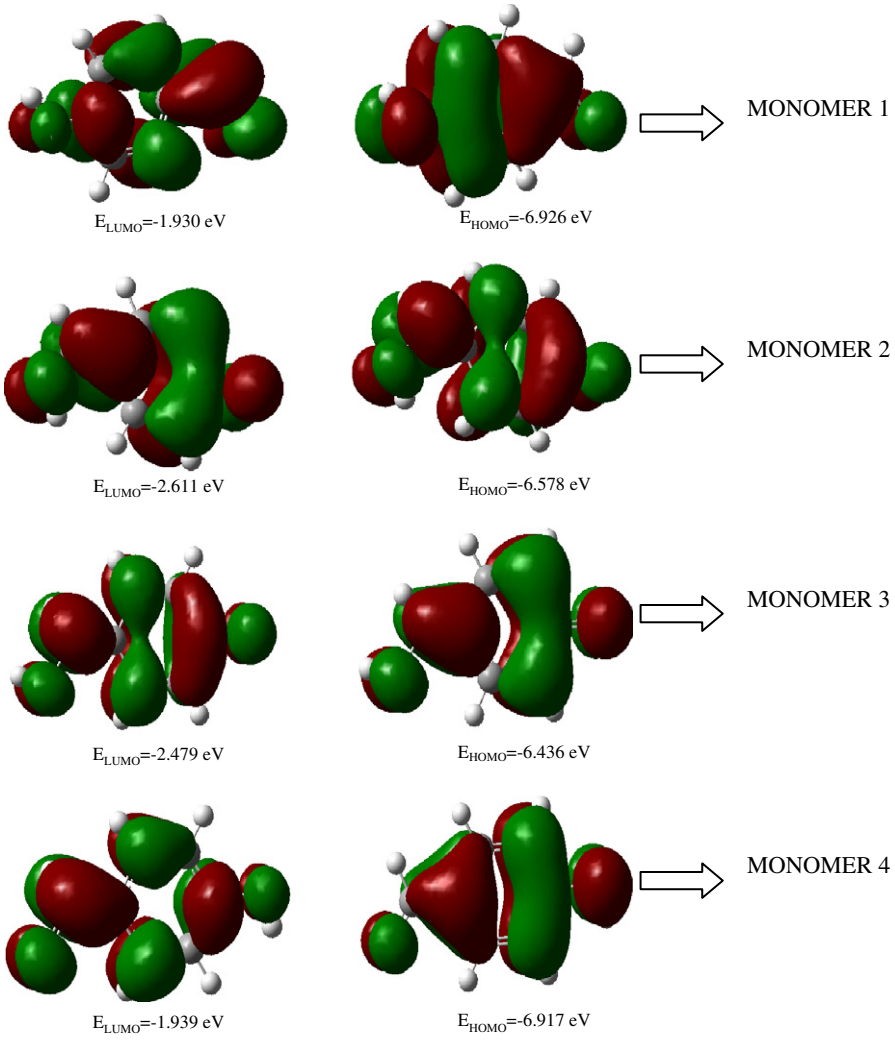

Fig. 6. HOMO–LUMO plot of PHBA monomer at B3LYP/6-31++G(d,p).

hyperpolarizability enhancement as reported earlier [42,43]. With donor substituents, the 19a mode in p-disubstituted benzene can be expected above 1500 cm^{-1} with higher intensity and 19b appears as weak band around 1400 cm^{-1} [38–41]. The vibrational modes 19a, 19b and 14 are computed at 1494 cm^{-1}, 1425 cm^{-1} and 1333 cm^{-1}, respectively. The modes corresponding to 19a can be found at 1518 cm^{-1} in IR spectrum. 19b can be observed as a weak band at 1423 cm^{-1} in IR spectrum and the corresponding band in Raman are very weak at 1422 cm^{-1}. Vibration 14 can be observed as a strong band in IR at 1315 cm^{-1} and as a medium band in Raman at 1315 cm^{-1} and the ring mode are coupled with H_{13}–O_{10}–C_4 in-plane bending. It is evident that the intermolecular interactions are not affecting the band positions of the tangential C–C stretching vibrational modes. The simultaneous activation of ring C–C stretching modes 8 and 14 provide apparent evidence for the charge transfer interactions [42,43].

In p-disubstituted benzene the phenyl modes 3, 15, 18a and 18b have been reported to have C–H in-plane bending character and can be expected in the region 1300 cm^{-1}–1000 cm^{-1}. The mode 3 appears as strong band in IR at 1284 cm^{-1} and in Raman at 1286 cm^{-1}. The strong band observed in IR at 1217 cm^{-1} and a medium band appears in Raman at 1218 cm^{-1} is assigned to the vibrational mode 15. The IR bands observed at 1159 and 1113 cm^{-1} are assigned to the 18a and 18b mode, respectively. The mode 18a appears in Raman at 1163 cm^{-1}. These assignments are in agreement with values given in the literature [38–40].

The absorption bands arising from C–H out-of-plane bending vibrations are usually observed in the region at 1000–675 cm^{-1} [38–40]. The C/H out-of-plane deformation result from b_{2g} (985 cm^{-1}), e_{2u} (970 cm^{-1}), e_{1g} (850 cm^{-1}) and a_{2u} (671 cm^{-1}) modes of benzene. The in-planar carbon bending vibrations are derived from non-degenerate b_{1u} (1010 cm^{-1}) and degenerate e_{2g} (606 cm^{-1}) modes of benzene. The C–H out-of-plane vibrations and ring breathing modes (1, 12, 6a and 6b) are shown in Table 3. This is in good agreement with literature values [38–41].

4.6. First-order molecular hyperpolarizabilities of p-hydroxybenzaldehyde monomer and dimer

The first-order molecular hyperpolarizability (β_0) of this novel molecular system, and related properties (β, α_0 and $\Delta\alpha$) of PHBA are calculated using HF/6-31++G(d) basis set, based on the finite-field approach. In the presence of an applied electric field, the energy of a system is a function of the electric field. First hyperpolarizability is a third rank tensor that can be described by a $3 \times 3 \times 3$ matrix. The 27 components of the 3D matrix can be reduced to 10 components due to the Kleinman symmetry [44]. The components of β are defined as the coefficients in the Taylor series expansion of

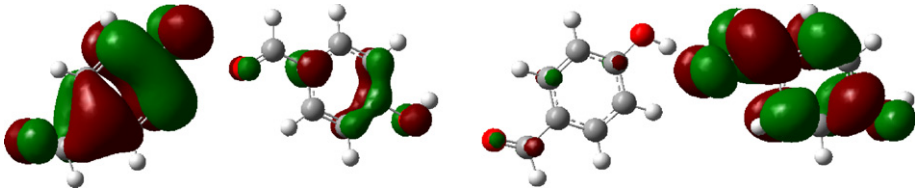

Fig. 7. HOMO–LUMO plot of PHBA dimer at B3LYP/6-31++G(d,p).

the energy in the external electric field. When the external electric field is weak and homogeneous, this expansion becomes,

$$E = E_0 - \sum_i \mu_i F^i - \frac{1}{2}\sum_{ij} \alpha_{ij} F^i F^j - \frac{1}{6}\sum_{ijk} \beta_{ijk} F^i F^j F^k - \frac{1}{24} \times \sum_{ijkl} \gamma_{ijkl} F^i F^j F^k F^l + \cdots \quad (2)$$

where E_0 is the energy of the unperturbed molecules, F^i is the field at the origin μ_i, α_{ij}, β_{ijk} and γ_{ijkl} are the components of dipole moment, polarizability, the first hyperpolarizabilities, and second hyperpolarizabilities, respectively. The components of the hyperpolarizability tensor are shown in Table S1 (in supporting information). The calculated first hyperpolarizability of PHBA is predicted for the first time 3.749×10^{-30} esu and 1.1747×10^{-29} esu, for monomer and dimer, respectively.

The π-conjugated systems having large values of molecular second-order polarizabilities (β), were analyzed with the help of vibrational spectroscopy [42,43,45]. The peculiar features observed in Raman and infrared spectra are simultaneous activation of some of the vibrational modes. The experimental behavior is well accounted by *ab initio* calculations in π-conjugated molecules that predict exceptionally large Raman cross-sections and infrared intensities for the same normal modes. Selection rule predicts the splitting of vibrational mode 8 in p-disubstituted phenyl ring and the vibrational mode 8a possesses higher wavenumber. No such splitting can be observed in IR and Raman spectra of PHBA, contradicting the selection rule. Also the bands at 1665 cm^{-1}, 1593 cm^{-1}, 1452 cm^{-1}, 1315 cm^{-1}, 1284 cm^{-1}, 1217 cm^{-1} and 1159 cm^{-1} observed in IR have their counterparts in Raman at 1665 cm^{-1}, 1586 cm^{-1}, 1451 cm^{-1}, 1315 cm^{-1}, 1286 cm^{-1}, 1218 cm^{-1} and 1163 cm^{-1}, respectively and their relative intensities in IR and Raman spectra are comparable.

The conjugated molecules are characterized by a small amount of highest occupied molecular orbital–lowest unoccupied molecular orbital (HOMO–LUMO) separation, which is the result of a significant degree of ICT from the end-capping electron-donor groups to the efficient electron-acceptor groups through π-conjugated path. The HOMO–LUMO energy gap for PHBA was computed at the B3LYP/6-31++G(d,p) level. The eigen values of LUMO and HOMO and their energy gap reflect the chemical activity of the molecule. Moreover the lower in the HOMO and LUMO energy gap explains the eventual charge transfer interactions taking place within the molecule. The atomic orbital compositions of the frontier molecular orbitals of PHBA monomer and dimmer are shown in Figs. 6 and 7.

5. Conclusions

The single crystals of PHBA have been grown by slow evaporation technique. The detailed interpretation of the vibrational spectra has been carried out with the aid of normal coordinate analysis (NCA) following the scaled quantum mechanical force field methodology. The various intramolecular interactions that is responsible for the stabilization of the molecule was revealed by natural bond orbital analysis. NIR-FT-Raman and FT-IR spectral studies reveals that the O–H stretching vibrational wavenumber is red-shifted owing to the formation of strong O–H···O hydrogen bonds by hyperconjugation between carbonyl oxygen lone electron pairs and O–H σ^* anti-bonding orbitals. The C–H stretching of aldehyde group interacts with the overtone of CH in-plane bending via Fermi Resonance. The lowering of HOMO and LUMO energy gap clearly explicates the charge transfer interactions taking place within the molecule.

References

[1] S.S. Gupte, A. Marcano, R.D. Pradhan, C.F. Desai, J. Melikechi, Appl. Phys. 89 (2001) 4939.
[2] S.P. Karna, J. Phys. Chem. A 104 (2000).
[3] D.R. Kanis, M.A. Ratner, T.S. Marks, Chem. Rev. 94 (1994) 195.
[4] H.S. Nalwa, S. Miyata, Nonlinear Optical Properties of Organic Molecules and Polymers, CRC Press, Boca Raton, FL, 1996.
[5] D.S. Chemla, J. Zyss, Non-linear Optical Properties of Organic Molecular Crystals, vols. 1 and 2, Academic Press, London, 1987.
[6] Peter Gunter (Ed.), Nonlinear Optical Effects and Materials, Springer-Verlag, Berlin, Heidelberg, New York, 2000.
[7] P.J.A. Ribeiro-Claro, L.A.E. Batista de Carvalho, A.M. Amado, J. Raman Spectrosc. 28 (1997) 867.
[8] N. Karger, A.M. Amorim da Costa, P.J.A. Ribeiro-Claro, J. Phys. Chem. A 103 (1999) 8672.
[9] P.J.A. Ribeiro-Claro, M.G.B. Drew, V. Felix, Chem. Phys. Lett. 356 (2002) 18.
[10] M.P.M. Marques, A.M. Amorim da Costa, P.J.A. Ribeiro-Claro, J. Phys. Chem. A 105 (2001) 5292.
[11] T. Schaeffer, K.J. Cox, R. Sebastian, Can. J. Chem. 69 (1991) 908.
[12] A. Anjaneyulu, G. Ramana Rao, Spectrochim. Acta A 55 (1999) 749.
[13] M.K. Aralakkanavar, N.R. Katti, P.R. Jeeragal, G.B. Kalakoti, R. Rao, M.A. Shashidhar, Spectrochim. Acta 48A (1992) 983.
[14] D.N. Singh, I.D. Singh, R.A. Yadav, Ind. J. Phys. 76B (1) (2002) 35.
[15] D.N. Singh, I.D. Singh, R.A. Yadav, Ind. J. Phys. 76B (3) (2002) 307.
[16] H. Lampert, W. Mikenda, A. Karpfen, J. Phys. Chem. A 101 (1997) 2254.
[17] H. Mollendal, S. Gundersen, M.A. Tafipolsky, H.V. Volden, Mol. Struct. 444 (1998) 47.
[18] A. Das, K. Kumar, J. Raman Spectrosc. 30 (1999) 563.
[19] L.D. Speakman, B.N. Papas, H.L. Woodcook, H.F. Schaefer, J. Chem. Phys. 120 (9) (2004) 4247.
[20] G.P. Kushto, P.W. Jagodzinski, Spectrochim. Acta 54A (1998) 799.
[21] G.P. Kushto, P.W. Jagodzinski, J. Mol. Struct. 516 (2000) 215.
[22] P.J.A. Ribeiro-Claro, M.P.M. Marques, A.M. Amado, Chem. Phys. Chem. 3 (2002) 599.
[23] Md. Qayyum, B. Venkatram Reddy, G. Ramana Rao, Spectrochim. Acta A60 (2004) 279.
[24] J.H.S. Green, D.J. Harrison, Spectrochim. Acta A 32 (1976) 1265.
[25] P. Bednarek, T. Bally, J. Gebicki, J. Org. Chem. 67 (2002) 1319.
[26] D. Sajan, J. Binoy, B. Pradeep, K. Venkata Krishna, V.B. Kartha, I. Hubert Joe, V.S. Jayakumar, Spectrochim. Acta A 60 (2004) 173.
[27] J. Binoy, Jose P. Abraham, I. Hubert Joe, V.S. Jayakumar, J. Aubard, O.F. Nielsen, J. Raman Spectrosc. 36 (2005) 63.
[28] D. Sajan, J. Binoy, I. Hubert Joe, V.S. Jayakumar, Jacek Zaleski, J. Raman Spectrosc. 36 (2005) 221.
[29] D. Sajan, I.H. Joe, J. Zaleski, V.S. Jayakumar, J. Mol. Struct. 785 (2006) 43.
[30] D. Sajan, G.D. Sockalingum, M. Manfait, I. Hubert Joe, V.S. Jayakumar, J. Raman Spectrosc. 39 (2008) 1772–1783.
[31] Jerry P. Jasinski, Ray J. Butcher, B. Narayana, M.T. Swamy, H.S. Yathirajan, Acta Cryst. E64 (2008) O187.
[32] M.J. Frisch, G.W. Trucks, H.B. Schlegel, G.E. Scuseria, M.A. Robb, J.R. Cheeseman, G. Scalmani, V. Barone, B. Mennucci, G.A. Petersson, H. Nakatsuji, M. Caricato, X. Li, H.P. Hratchian, A.F. Izmaylov, J. Bloino, G. Zheng, J.L. Sonnenberg, M. Hada, M. Ehara, K. Toyota, R. Fukuda, J. Hasegawa, M. Ishida, T. Nakajima, Y. Honda, O. Kitao, H. Nakai, T. Vreven, J.A. Montgomery Jr., J.E. Peralta, F. Ogliaro, M. Bearpark, J.J. Heyd, E. Brothers, K.N. Kudin, V.N. Staroverov, R. Kobayashi, J.

Normand, K. Raghavachari, A. Rendell, J.C. Burant, S.S. Iyengar, J. Tomasi, M. Cossi, N. Rega, J.M. Millam, M. Klene, J.E. Knox, J.B. Cross, V. Bakken, C. Adamo, J. Jaramillo, R. Gomperts, R.E. Stratmann, O. Yazyev, A.J. Austin, R. Cammi, C. Pomelli, J.W. Ochterski, R.L. Martin, K. Morokuma, V.G. Zakrzewski, G.A. Voth, P. Salvador, J.J. Dannenberg, S. Dapprich, A.D. Daniels, O. Farkas, J.B. Foresman, J.V. Ortiz, J. Cioslowski, D.J. Fox, Gaussian 09, Revision A.02, Gaussian Inc., Wallingford, CT, 2009.

[33] Listing of vibrational scaling factors. <http://srdata.nist.gov/cccbdb/vibscalejust.asp>.

[34] J. Baker, A.A. Jarzecki, P. Pulay, J. Phys. Chem. A 102 (1998) 1412.

[35] G. Keresztury, S. Holly, J. Varga, G. Besenyei, A.Y. Wang, J.R. Durig, Spectrochim. Acta A 49 (1993) 2007.

[36] G. Keresztury, in: J.M. Chalmers, P.R. Griffith (Eds.), Raman Spectroscopy: Theory in Handbook of Vibrational Spectroscopy, vol. 1, John Wiley & Sons Ltd., New York, 2002.

[37] A.E. Reed, L.A. Curtiss, F. Weinhold, Chem. Rev. 88 (1988) 899.

[38] D.L. Vein, N.B. Colthup, W.G. Fateley, J.G. Grasselli, The Handbook of Infrared and Raman Characteristic Frequencies of Organic Molecules, Academic Press, New York, 1991.

[39] N.B. Colthup, L.H. Daly, S.E. Wiberley, Introduction to Infrared and Raman Spectroscopy, Academic Press, New York, 1990.

[40] G. Socrates, Infrared and Raman Characteristic Group Frequencies: Tables and Charts, third ed., Wiley, Chichester, 2001.

[41] G. Varsanyi, Vibrational Spectra of Benzene Derivatives, Academic Press, New York, 1969.

[42] C. Castiglioni, M. Del Zoppo, P. Zuliani, G. Zerbi, Synth. Metal. 74 (1995) 171.

[43] M. Del Zoppo, C. Castiglioni, P. Zuliani, A. Razelli, M. Tommasini, G. Zerbi, M. Blanchard-Desce, J. Appl. Polym. Sci. 70 (1998) 1311.

[44] D.A. Kleinman, Phys. Rev. 126 (1962) 1977.

[45] C.H. Bosshard, R. Spreiter, L. Degiorgi, P. Gunter, Phys. Rev. B 66 (2002) 205107.